

A Machine Learning Method for Detecting Brain Tumour using Magnetic Resonance Images

Vikas Tripathi¹, Devvret Verma², Vrinca Vimal³

¹Department of Computer Science & Engineering, Graphic Era Deemed to be University, Dehradun, Uttarakhand India, 248002

²Department of Biotechnology, Graphic Era Deemed to be University, Dehradun, Uttarakhand India, 248002

³Department of Computer Science & Engineering, Graphic Era Hill University, Dehradun, Uttarakhand India, 248002

ABSTRACT

When it comes to brain tumours, gliomas are the most aggressive and potentially fatal kind because of their rapid growth. Due to their a typical appearance and porous tumor-normal boundary, gliomas make computer-aided treatment of these tumours a difficult task. The most common technique for imaging human brain patterns of concern is magnetic resonance imaging (MRI). In this research, we display a deep learning-based technique for brain tumor classification that makes use of multiple MRI modalities. When making predictions about the label of an input image, the proposed hybrid convolutional neural network architecture uses a patch-based method that incorporates both local and global features. In order to combat over-fitting, the proposed network makes use of a dropout regularization term in conjunction with batch normalisation, and it handles data imbalance via a two-stage training procedure. The proposed method begins with an image normalisation step that occurs during the processing phase. post-processing stage that corrects for bias in the feed-forward pass through a convolutional neural network (CNN) that was used to eliminate relatively insignificant false positives near the head's crown Results from running the proposed method upon that BRATS dataset show that it is effective, with mean squared error rates of Dice scores for the whole tumour region improved to 0.86, 0.89, and 0.93, respectively, from new, cutting-edge methods.

Keywords: Brain segmentation, CNN, Machine Learning, MRI

INTRODUCTION

Gliomas are the most prevalent and lethal kind of brain tumour [1]. Although high-grade astrocytoma's are extremely deadly, reduced gliomas (LGG) have been thought to be less so [2]. HGG patients have a two-year life expectancy at most, while LGG patients, based on tumour progression, can reside for years. Radiation therapy, chemo, and surgery are all methods that can be used to treat gliomas [1,3]. MRI has become the standard technique for imaging brain structures (MRI). MRI provides the most adaptable imaging technology for simulating brain specific areas of

interest, including malignancies, due to its flexibility to equalize cell contrast. The goal of tumour segmentation is to correctly divide voxels that exhibit features typical of tumours, such as edoema, necrotic centres, and metastatic tumor tissues [4]. Due to their infiltrative nature, gliomas' fuzzy limits make them difficult to spot in images with varying intensities. The problem of varying intensities [6] arises because of the wide range of MRI machine setups available today (1.3, 5 or 7 T). Numerous MRI methods are utilised to enhance the information extracted from MR images. Using these modalities, one can obtain various kinds of information about tumour pixels, such as T1w spin-lattice relieving stress (T1), T2-weighted spin-spin loosening (T2), T1-weighted Myocardial infarction with observably (T1c), and T2-weighted MRI with fluid damping reversal recovery (T2flair) [6]. Different intensities and patterns are provided by different methods for the same tumour area. This facilitates the process of discovering associations between the various tumour types visible in the picture. The T1 and T1c modalities produce images with higher brightness and contrast, while the T2 and T2flair modalities produce images with darker shading to highlight the tumor's structure. This improves the model's ability to recognise multiple patterns within the image pixels, which in turn facilitates the detection of diffuse tumour regions and structure irregularities. For accurate tumour growth prediction and treatment strategy development, MR image classification of brain tumours is invaluable [7]. However, manually segmenting tumour images is a time-consuming task, despite the fact that glioma tumour segmentation can be of great help in CAD. An increasing number of healthcare centres are generating brain images of tumours every day, and each MRI has between 150 and 220 slices. There is a risk of fatal outcomes because doctors are relying on estimates and intuition when diagnosing a patient with a tumour [2]. Both the complexity and practicality of the automatic segmentation in the healthcare setting have led to the development of numerous automated and semiautomated methods for detecting and segmenting tumours to aid in diagnostic procedures [8]. Because of their unpredictable growth and atypical appearance, brain tumours present significant challenges for automated tumour detection [9]. Most previous techniques have been evaluated using manually crafted datasets, making it impossible to know how well they would fare in a more general setting. The Medical Imaging Computation and Computer-Assisted Therapy Society is responsible for the collection and distribution of scan data libraries (MICCAI). Subsequently, these values have been utilised as a benchmark against which to judge brand-new approaches and algorithms that have been developed. The material that was used to test how effective the proposed method was was derived from a challenge involving the segmentation of neurological disorders. In this paper, we investigate a variety of CNN architectures by experimenting with different configurations of stacked convolution. While sectioning brain MRI, the classifiers that rely on hand-crafted features ignore label dependencies. Convolutional neural networks (CNNs) use the kernels in convolution layers to account for neighbouring labels. The neighbourhood of a pixel, which will be taken into account when predicting the yield label for that pixel, is set by the length of the kernels. In furthermore to CNNs' value, a combination model is proposed that brings together the best features of the two-path and three-path models.

When these networks are combined, the surrounding pixels have a greater impact on the predicted results, which is based on contextual and local features. The former describes data about the immediate surroundings of the target pixel, while the latter describes data about the entire frame or a bigger region. Because pixels that are adjacent to one another often belong to the same class, local information is vital. Global knowledge, on the other hand, provides an overall background to a

particular target class. The approach being presented makes use of smaller kernels (2*2) in the convolution operation in order to extract location features, while it makes use of bigger kernels (12*12) in order to extract relevant data. The performance of the proposed algorithm is evaluated on the BRATS dataset by generating 2D patches employing a patch-based approach. On this dataset, the suggested algorithm achieves better results than state-of-the-art techniques.

RELATED WORK

Numerous automated brain tumour segmentation methods are proposed to aid CAD [10], indicating that the field of tumour segmentation is still extremely active for research. When it comes to MRI, brain tumour segmentation algorithms can be broken down into two broad categories. The algorithms can be thought of as either generative as well as discriminative models [11]. The ability of generative models to distinguish between normal and malignant voxels is predicated on having this prior knowledge. Automation of tumour tissue classification is difficult because of their irregular shapes. The voxels that make up the tumour are flagged as abnormal by the generative models. Most of the time, atlases and other anatomy models are used to construct these simulations [12]. Prastawa et al. provides a good illustration of a generative model by comparing a query image to an ICBM brain atlas and calculating the posterior probabilities of three major brain regions (white matter, grey matter, and spinal fluid). A limit is then used to identify low-probability tumour pixels by comparing voxels to it. Through a process of post-processing, the unique regularity is preserved. Both Khotanlou et al. and Popuri et al. [13] propose numerous atlas-based techniques for determining the tumour region probabilities. These techniques have made use of the symmetric nature of the brain to perform computations. The tumour region is represented by the lowest probability value, and the probabilities have been calculated by starting an active contour and iterating until that value is reached. Tumor segmentation and atlas register have both been accomplished by some of the techniques.

Rather than being specifically adapted to the brain tumour field, numerous discriminative methods rely on generalised edge-based data. Recently, deep learning-based algorithms [14,15,16] have been employed to complete the task of brain tumor classification due to their efficacy in recognising patterns in images. Classifying the centre pixel in MR images is a common practise for current CNN-based algorithms [17]. Successful applications of CNNs include scene classification [18], tissue classification [19], and semantic segmentation [20]. Jiang et al. [21] suggest using two convolutional neural network (CNN) based classifiers to separate tumour pixels from healthy ones. In order to perform well, such models need to be fine-tuned by hand for each test image in the dataset. Rao et al. [22] was using a hybrid version involving CNN and RF, in which a picture was fed into a trained CNN to extract a feature vector, that was then fed into the RF algorithm to generate predictions. In their paper, Saouli et al. [23] introduce the idea of ensemble learning, wherein two neural network-based models are combined and results are aggregated incrementally. Since neural networks present an exciting new possibility for medical segmentation, the above study investigates a CNN-based approach to classifying MR image pixels into one of five categories.

PROPOSED METHODOLOGY

As can be seen in Fig. 1, the suggested technique consists of three major phases preprocessing, a convolutional neural network (CNN), and post-processing. The following section elaborate on the

various steps of such proposed method.

3.1 Pre-processing

MR images may pick up artefacts like bias field distortion and motion heterogeneity due to subject motion or the constraints of a MRI machine. These artefacts cause false positives in segmented images by inducing false intensity values. N4ITK, an enhanced form of the nonparametric, nonuniform intensity normalisation (N3) [24], is used to correct for biases that cause such artefacts. The BRATS dataset has inconsistent third-dimensional resolutions, so 3D MR images are flattened into 2D slices. Accordingly, the proposed method employs uniformly sized axial slices. Due to the varying intensity values in such slices, CNN has a hard time tailoring its features to a specific class label. By bringing the intensities values contained within the dataset into a uniform range with a median pixel intensity around 0 and a standard deviation near one, the normalizing procedure helps users deal with intensity changes. To produce output i_0 , the input slice I is normalised in terms of average and standard deviation, as

$$i_0 = \frac{i - \mu}{\sigma} \quad (1)$$

Just after segments are normalised, the final step is to normalise the spots of size $N \times N$ that will be used for training and evaluation so that they have zero mean and unit variance.

3.2 Convolutional Neural Networks

When it comes to identifying patterns across a wide range of image formats, CNNs have shown to be extremely efficient [43]. A typical CNN consists of input, a convolutional, a max pooling layer, a densely integrated (FC) layer, and an output layer. The layer is pivotal in a neural network convolutional since it is responsible for identifying patterns and attributes in input pictures using convolved kernels. Different sizes of filters (3 x 3, 7 x 7, and 13 x 13 are all examples of CNN kernels) are combined out over information to create a feature map in a sliding window fashion.

For every position on a feature space has a weighted connection to the output of the layer below it based on the feature's importance. When learning a network, back-propagation [44] is used to adjust the connection weights after each mini-batch of data has been processed by the system. The layers are quicker than FC layers because their fewer weights allow a kernel to handle an entire map. Features in a convolution layer are represented by neurons, and each neuron's value is established by the pixels immediately around it. The term "responsive field" [45] describes the area of pixels that actually potentially influence the neuron's activation. The size of a neuron's perceptron grows with the number of convolution layers superimposed on it. The conv layer's perceptron is affected by the kernel size since it is used to determine the surrounding pixels. Increasing the size of the kernel causes more of the surrounding neurons to fire, enriching the feature map with additional contextual details. The feature mapping Calculating f_{aj} looks like this:

$$f_{aj} = b_a + \sum_{n=1}^{\infty} K_{aJ} * I_j \quad (2)$$

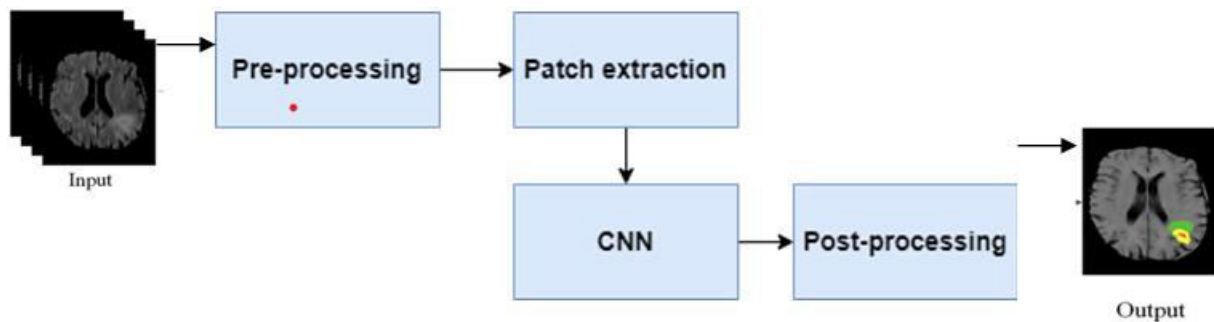


Fig 1: Block diagram of the Proposed Methodology

3.2.1 Two-Path CNN

The input is split between two different nodes in the network to build the two-path, as depicted. The first stream makes use of narrow-receptive-field kernels to extract local features from the image, while the second stream employs wide-receptive-field kernels to extract contextual details. The network utilises two max - pooling in the first stream that follows the convolution layers and makes use of four convolution layers. The output of the last convolution layer is a combined map from all the streams, and the output of the FC layer is a combined 1D vector from all the feature maps. The max pooling overlay is used to further compress the sparse representations obtained via Activation functions. This model is quicker than the more complex three-path model because there are fewer flows to process. When dealing with the issue, a dropout of 0.5 is used in the first few model layers and gradually decreases as the network gets more complex.

A convolutional neural networks (CNN) levels can be organised in a variety of ways, including in parallel and in a linear fashion. Two networks with different capabilities can be combined to create a hybrid model by concatenating the output of multiple convolution layers. Following this section is a breakdown of the various architectural layouts that were considered for this study.

3.2.2 Three-Path CNN

The three-path CNN network is made up of 3 parallel layers that are combined by a convolution layer. Several features can be detected with the help of the parallel paths' use of varying convolution kernels. Since the depth the network, more the variables per layer, the fewer convolution kernels can be used effectively. In total, the network employs 5 convolution layers, with 1 pooling layer deployed in the third data stream. Due to its large receptive field, this prototype is more precise than the alternative two-path model. Throughout this model, the over-fitting issue is addressed with a drop - outs of 0.5 and the kernel maps produced by the convolution layers are activated with ReLU. 3 streams' output is combined in the final convolution, and a flatten layer is used to transform 2D into a single 1D feature vector. The above network's FC uses 380 features to determine the probability of five different classes of output.

3.2.3 Hybrid CNN

In order to combine the advantages of both 2- and 3-path CNNs, we employ the concatenating capabilities of the convolution layers to produce a hybrid model, as shown in Fig. 2. Through fusing the sensitivities of two CNNs, the hybrid network is better able to learn a wide variety of features

while also considering the global and local environments. This network overcomes a major shortcoming of 2 and 3 path networks by modelling local dependencies between output labels; these networks need not consider labels in the immediate vicinity of the expected label. The final feature is calculated by concatenating the output of two- and three-path networks and convolving them with 2×2 kernels in the hybrid convolution before output nodes. More information about dependencies among labels is included in the final maps because they are built from the outcome of two networks. Despite having 9 convolution layers, the network is fast because most of the work is performed in parallel. The network's efficiency and effectiveness rely on the 380 features sent to the FC layer.

3.3 post-processing

Because of the extreme intensity near the skull region of the throughput segmentation, some minor false positives appear there. The proposed method culminates in the use of morphological operations to refine the segmentation results by evacuating stray false positives from the expected output's margins. False positives are eliminated via erosion, a straightforward procedure, and the output is expanded via dilation, a more complex procedure. In post-processing, the deterioration and expansion known as opening operation is utilised.

EXPERIMENTAL SETUP

The sections that follow describe the data, experimental parameters, and training phase that were used to develop the proposed CNNs.

4.1 Dataset

BRATS (Multimodal Brain Tumor Segmentation Challenge) [14] hosts the BRATS dataset that is used to test the proposed method. T1, T2, T1c, T2flair, and the target label are the 4 MRI modalities included in the training dataset. Twenty high-quality hand-drawn geometric (HGG) and ten low-quality hand-drawn geometric (LGG) 3D training images with 155 2D slices each are included in the dataset. As extreme intensity in the skull area can lead to false positives, the info are preprocessed to remove skull stripes.

In the dataset, there are 5 types of output classes: healthy patches, edoema, nonenhancing tumour, enhancing tumour, and necrosis. 3 cumulative classes are used to verify the proposed method: the enhancing tumour class, the core tumour class, and the complete tumour class. In this paper, the green colour stands for the numerical class 2 that represents tumour growth promotion. Red, blue, and yellow stand for classes 1, 3, and 4 in a tumor's core, while all four classes are represented by the tumor's whole.

4.2 Implementation details

Keras [47] machine learning, an elevated library with many tools for putting deep learning algorithms into action, is used to carry out the proposed method. It's compatible with the TensorFlow and Theano backends, and it comes with a plethora of pre-trained networks that utilize GPU and CPU processing capacity. Grid search algorithm is employed to adjust the network's hyperparameters; it's indeed similar to cross-validation algorithm but is applied to adjusting network parameters rather than model parameters utilising training and validation data. The tumour

segmentation problem is most effectively solved using the stochastic gradient descent (SGD) algorithm in conjunction with the ReLU activation. The values are initially zero for the convolution layer kernels and 0.3 for the output nodes. In order to create feature maps that are insensitive to translation, we set the stride to 1 for all of the max pooling and convolution layers. Figures depict the optimal values for the proposed network's variables. On the testing set, the network excels with these settings. The BRATS dataset's axial slices are used to create 25x25px patches that are split 70:30 between a training set or an evaluation set. Unfortunately, only 10% of the training examples is utilized in the validation set. Over-fitting is a typical problem in deep learning whenever the number of training samples is low. As a result of using 200,000 patches to training the system, dropout and other regularises are necessary to prevent over-fitting. Dropout is set at 0.5 for the first several levels of the network and 0.25 for the last layer of the model.

Evaluation metrics

Dice score coefficient (DSC), sensitivity, and specificity [14] are used to verify the efficacy of the proposed algorithm.

$$DSC = 2 \times \frac{|M \cap N|}{|M| + |N|} \quad (4)$$

where M and N reflect the throughput label and the expected segmentation, in both, and the DSC represents the overlap between the two.

Sensitivity is the measure of true positives and characterises how precisely a tumour can be located in an image.

$$\text{Sensitivity} = \frac{|N \cap M|}{|M|} \quad (5)$$

$$\text{Specificity} = \frac{|N_o \cap M_o|}{|M_o|} \quad (6)$$

where N_o and M_o are the predicted true negatives and the labelled true negatives, respectively, defines an algorithm's capacity to predict healthy pixels, i.e., the precision of true negatives in an MR image.

EXPERIMENTAL RESULTS AND DISCUSSION

The BRATS dataset is used for the experiments, which are conducted on actual patient data. Due to the low resolution of the images in 3D, the MR photos in the dataset were transformed to 2d images. Axisymmetric view is used to extract the patches because of its uniform dimensions, while labels are only used for model training. The dataset includes four image methods (T1, T2, T1c, and T2flair), which are used to train the configurations. Detection-Selectivity-Calibration (DSC), detection sensitivity, and detection specificity are the 3 performance indicators used to notify the experimental data. Subsequent sections give more detail on the implications of two-phase training and parallel layer arrangements.

5.1 Two path network

As its name implies, the two-path system takes advantage of two independent paths to glean regional and international data. Fig. 7 is a visual representation of the results for the two-path network. To address the issue of data inconsistency, a two-stage training procedure is used to educate the network. Learning a linear single-path model first, which performs poorly across all tumour regions, demonstrates the efficacy of employing a two-path network. The result of the tumour regions for this linear model performed at the best DSC levels of 0.8, 0.75, and 0.68, respectively. Table 1 shows that the two-path model outperforms the single-path model across all important measures of performance. The model performs better for core and enhancing regions than for the full tumour region because edema often has low intensity values throughout tumour voxels, dissolving it with good skin. The model does particularly well for core and enhancing regions, where edema is not present, and the resultant entire tumour dice score is lower than for other regions. The model outperforms the linear architecture, which struggles to deal with the complexity of the brain tumour segmentation problem, because it incorporates both global and regional information at the pixels.

5.2 Three path network

When 3 distinct paths are used, a more complex structure is created than the basic two-path network. In order to extract as much information as possible about the output label, the network uses three different convolution kernels of varying sizes. Also employing ReLU activation on the feature maps, the 3 network is trained with a two-stage training procedure. Table 1 displays the quantitative outcomes attained by employing a three-path network. Due to edema's difficult detection and fuzzy limits, the model is more effective for identifying core and enhancing regions than the entire tumour. We see a visual representation of the outcomes that can be expected from a three-path architecture.

The model picks up a wide range of features thanks to the network's three distinct convolution kernels in its first layer. The low-level features representation learned by network's three paths is depicted.

The bigger kernels extract worldwide data on the location and likelihood of tumour pixels in a given area, while the smaller kernels learn edge and boundary information.

5.3 Hybrid network

When the two- and three-path networks are combined, the resulting hybrid model outperforms both of them in every metric. To generate the final feature representation, the network uses a convolution layer to incorporate the feature maps generated by the two- and three-path networks. Since the final vertex is the result of multiplying the receptive fields of two networks, it contains both local and global details. The hybrid network is trained using a two-stage training algorithm, the outcomes of which are displayed in Fig. 10 for HGG and LGG, respectively. Fig. 11 displays the results of an additional processing step. In the absence of post-processing, the MRI scan might produce a few false positives near the image's borders; this problem is solved by adjusting the contrast and brightness of the image. Table 2 displays numerical results of the hybrid model in comparison to HGG and LGG. With both HGG and LGG gliomas, the model provides satisfactory results. When

comparing LGG and HGG, where the tumour labels are more evenly distributed, it is seen that the large percentage of labels in LGG tumour belong to the edoema and nonenhancing tumour, leading to significantly reduced DSC values. Training the network in two stages yields substantial gains across the board. With the network's ability to learn features from all output classes equally well, the disadvantage in edoema prediction seen in two- and three-path architectures is greatly reduced or eliminated.

Table 1: Results achieved by proposed networks on the dataset

Networks	DSC			Sensitivity			Specificity		
	Complete	Core	Enhancing	Complete	Core	Enhancing	Complete	Core	Enhancing
Two - path	0.75	0.82	0.83	0.79	0.82	0.83	0.9	0.9	0.9
Three - path	0.71	0.85	0.8	0.8	0.85	0.84	0.92	0.91	0.89
Hybrid	0.79	0.84	0.86	0.84	0.9	0.89	0.91	0.92	0.93

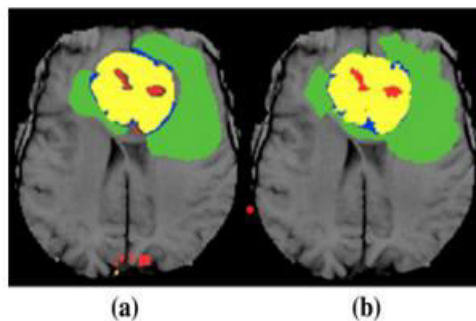


Fig 2: Result achieved by a two-path network

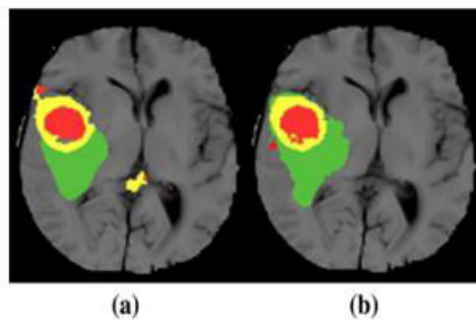


Fig 3: Result achieved by a three-path network

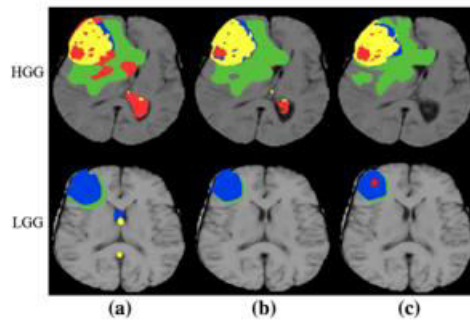


Fig 4: Result achieved by a hybrid network

CONCLUSION

Computerized segmentation of brain is crucial for glioma patients receiving computer-assisted diagnosis. In this study, we present a new automated hybrid version for tumor segmentation, which significantly improves upon the efficiency of previous methods. The hybrid model uses deep neural networks and heterogeneous MRI data to segment MR pictures from the BRATS database. It has been shown that the hybrid version, created by combining 2- and 3-path CNNs, outperforms the state-of-the-art approaches on all of the most relevant performance criteria. By using an update strategy, the suggested network dissects the developing brain by labelling the centre pixel of each patch. The result classes are predicted using both locally and globally observed data, and label linkages between pixels are taken into account. To deal with unbalanced data and guarantee that the proposed model is learning from the real distribution of labels, it employs a two-stage training procedure. To combat over-fitting, the proposed method makes use of a dropout regularize and other cutting-edge developments in data pre-processing, bias field correction. Various segmentation tests have demonstrated the usefulness of the suggested system, and its performance can be further improved by enhancing the number of training samples.

REFERENCE

1. Pereira, S.; Pinto, A.; Alves, V.; Silva, C.A.: Brain tumor segmentation using convolutional neural networks in MRI images. *IEEE Trans. Med. Imaging* 35(5), 1240–1251 (2016)
2. Bauer, S.; Wiest, R.; Nolte, L.-P.; Reyes, M.: A survey of MRIbased medical image analysis for brain tumor studies. *Phys. Med. Biol.* 58(13), R97 (2013)
3. Tabatabai, G.; Stupp, R.; van den Bent, M.J.; Hegi, M.E.; Tonn, J.C.; Wick, W.; Weller, M.: Molecular diagnostics of gliomas: the clinical perspective. *Acta Neuropathol.* 120(5), 585–592 (2010)
4. Zhao, X.; Yihong, W.; Song, G.; Li, Z.; Zhang, Y.; Fan, Y.: A deep learning model integrating FCNNs and CRFs for brain tumor segmentation. *Med. Image Anal.* 43, 98–111 (2018)
5. Havaei, M.; Davy, A.; Warde-Farley, D.; Biard, A.; Courville, A.; Bengio, Y.; Pal, C.; Jodoin, P.-M.; Larochelle, H.: Brain tumor segmentation with deep neural networks. *Med. Image Anal.* 35, 18–31 (2017)
6. Abbasi, S.; Pour, F.T.: A hybrid approach for detection of brain tumor in MRI images. In: 2014 21th Iranian Conference on Biomedical Engineering (ICBME), pp. 269–274 (2014)

7. Kao, P.-Y.; Ngo, T.; Zhang, A.; Chen, J.; Manjunath, B.S.: Brain tumor segmentation and tractographic feature extraction from structural MR images for overall survival prediction (2018). arXiv preprint arXiv:1807.07716
8. Farahani, K.; Menze, B.; Reyes, M.; Gerstner, E.; Kirby, J.; Kalpathy-Cramer, J.: Multimodal Brain Tumor Segmentation (BRATS 2013). <http://martinos.org/ctim/miccai2013> (2013)
9. Hussain, S.; Anwar, S.M.; Muhammad, M.: Brain tumor segmentation using cascaded deep convolutional neural network. In: 2017 39th Annual International Conference of the IEEE Engineering in Medicine and Biology Society (EMBC), pp. 1998–2001 (2017)
10. Bernal, J.; Kushibar, K.; Asfaw, D.S.; Valverde, S.; Oliver, A.; Martí, R.; Lladó, X.: Deep convolutional neural networks for brain image analysis on magnetic resonance imaging: a review. *Artif. Intell. Med.* 95, 64–81 (2018)
11. Pinto, A.; Pereira, S.; Correia, H.; Oliveira, J.; Rasteiro, D.; Silva, C.A.: Brain tumour segmentation based on extremely randomized forest with high-level features. In: 2015 37th Annual International Conference of the IEEE Engineering in Medicine and Biology Society (EMBC), pp. 3037–3040 (2015)
12. Doyle, S.; Vasseur, F.; Dojat, M.; Forbes, F.: Fully automatic brain tumor segmentation from multiple MR sequences using hidden Markov fields and variational EM. *Proc. NCI-MICCAI BRATS 1*, 18–22 (2013)
13. Popuri, K.; Cobzas, D.; Murtha, A.; Jägersand, M.: 3D variational brain tumor segmentation using Dirichlet priors on a clustered feature set. *Int. J. Comput. Assist. Radiol. Surg.* 7(4), 493–506 (2012)
14. Menze, B.H.; Jakab, A.; Bauer, S.; Kalpathy-Cramer, J.; Farahani, K.; Kirby, J.; Burren, Y.; Porz, N.; Slotboom, J.; Wiest, R.; et al.: The multimodal brain tumor image segmentation benchmark (BRATS). *IEEE Trans. Med. Imaging* 34(10), 1993–2024 (2015)
15. Urban, G.; Bendszus, M.; Hamprecht, F.; Kleesiek, J.: Multi-modal brain tumor segmentation using deep convolutional neural networks. In: *Proceedings of BRATS-MICCAI* (2014)
16. Beers, A.; Chang, K.; Brown, J.; Sartor, E.; Mammen, C.P.; Gerstner, E.; Rosen, B.; Kalpathy-Cramer, J.: Sequential 3D U-nets for biologically-informed brain tumor segmentation (2017). arXiv preprint arXiv:1709.02967
17. Zikic, D.; Ioannou, Y.; Brown, M.; Criminisi, A.: Segmentation of brain tumor tissues with convolutional neural networks. In: *Proceedings MICCAI-BRATS*, pp. 36–39 (2014)
18. Hu, J.; Mou, L.; Schmitt, A.; Zhu, X.X.: Fusionet: a two-stream convolutional neural network for urban scene classification using polsar and hyperspectral data. In: *Urban Remote Sensing Event (JURSE), 2017 Joint*, pp. 1–4 (2017)
19. Hou, L.; Samaras, D.; Kurc, T.M.; Gao, Y.; Davis, J.E.; Saltz, J.H.: Patch-based convolutional neural network for whole slide tissue image classification. In: *Proceedings of the IEEE Conference on Computer Vision and Pattern Recognition*, pp. 2424–2433 (2016)
20. Chen, L.-C.; Papandreou, G.; Kokkinos, I.; Murphy, K.; Yuille, A.L.: Deeplab: Semantic image segmentation with deep convolutional nets, Atrous convolution, and fully connected CRFs (2016). arXiv preprint arXiv:1606.00915

21. Jiang, J.; Yao, W.; Huang, M.; Yang, W.; Chen, W.; Feng, Q.: 3D brain tumor segmentation in multimodal MR images based on learning population- and patient-specific feature sets. *Comput. Med. Imaging Graph.* 37(7), 512–521 (2013)
22. Rao, V.; Shari Sarabi, M.; Jaiswal, A.: Brain tumor segmentation with deep learning. In: *MICCAI Multimodal Brain Tumor Segmentation Challenge (BraTS)*, pp. 56–59 (2015)
23. Saouli, R.; Akil, M.; Kachouri, R.; et al.: Fully automatic brain tumor segmentation using end-to-end incremental deep neural networks in MRI images. *Comput. Methods Programs Biomed.* 166, 39–49 (2018)
24. Tustison, N.J.; Avants, B.B.; Cook, P.A.; Zheng, Y.; Egan, A.; Yushkevich, P.A.; Gee, J.C.: N4ITK: improved N3 bias correction. *IEEE Trans. Med. Imaging* 29(6), 1310–1320 (2010)